Microscopic modeling of confined crystal growth and dissolution

Jørgen Høgberget,[1] Anja Røyne,[1] Dag K. Dysthe,[1] and Espen Jettestuen[2,1]
[1]*Department of Physics, University of Oslo, N-0316 Oslo, Norway*
[2]*IRIS AS, P.O. Box 8046, N-4068 Stavanger, Norway*
(Received 9 November 2015; revised manuscript received 8 June 2016; published 16 August 2016)

We extend the (1+1)-dimensional fluid solid-on-solid (SOS) model to include a confining flat surface opposite to the SOS surface subject to a constant load. This load is balanced by a repulsive surface-surface interaction given by an ansatz which agrees with known analytical solutions in the limit of two separated flat surfaces. Mechanical equilibrium is imposed at all times by repositioning the confining surface. By the use of kinetic Monte Carlo (KMC) we calculate how the equilibrium concentration (deposition rate) depends on the applied load, and find it to reproduce analytical thermodynamics independent of the parameters of the interaction ansatz. We also study the dependency between the surface roughness and the saturation level as we vary the surface tension, and expand on previous analyses of the asymmetry between growth and dissolution by parametrizing the linear growth rate constant for growth and dissolution separately. We find the presence of a confining surface to affect the speed of growth and dissolution equally.

DOI: 10.1103/PhysRevE.94.023005

I. INTRODUCTION

Both confinement and elastic stress alter phase equilibria of liquids and solids [1,2]. The fundamental thermodynamics and out of equilibrium processes of stressed solids [3,4], confined systems [1], and combined effects of confinement and elastic stresses are interesting in their own right and they have important applications in metal alloying [2], growth of semiconductor heterostructures [5,6], frost heave [7], weathering of rocks and concrete [8–12], and metamorphism, diagenesis, and weathering in the Earth's crust [13,14].

Elastic strain energy in the solid is known to cause instabilities during freezing and growth or melting and dissolution, such as the Asaro Tiller Grinfeld (ATG) instability [15–18], precipitate growth instabilities in binary alloys [2], or Stranski-Krastanof growth in epitaxial growth of semiconductor heterostructures [4]. Another mode of stress transmission to the solid—normal to the solid-liquid interface—requires that the liquid layer confined between two solid surfaces transmits stress, a remarkable effect of confinement predicted by the Derjaguin Landau Vervey Overbeek (DLVO) theory [19,20] that has been amply demonstrated experimentally [1,7,21] and in molecular simulation [22]. The thermodynamics and out of equilibrium processes involving the coupling of phase transitions and normal stress from one solid through a confined liquid to another solid—from now on abbreviated *confined and stressed liquid-solid processes*—have been studied experimentally [11,14,23–25], thermodynamically [14,26,27], and by molecular simulation [28–30]. We have shown experimentally that confinement and stress cause instabilities during dissolution [31] and growth [32], phenomena that are yet to be studied by simulation or explained theoretically.

Recent studies show that the level of confinement is crucial when it comes to deciding the properties of the confined fluid such as the slip length, velocity field [33], and the dielectric constant [34]. Moreover, simulations indicate that the nature of the surface-solution interaction is very important when it comes to nucleation within small channels [30]. It is also known that entropic effects in confinement, i.e., the finite-size effects, are very important when deciding the properties of growing surfaces [35–37]. However, little attention has been given to the normal stress induced by the surface-surface interactions in these confined environments. One reason for this is that due to their detailed description of the fluid and the fine temporal resolution required to resolve atomic vibrations, typical molecular simulation techniques such as molecular dynamics are not well suited for modeling growth or dissolution on crystal surfaces, which occurs over larger times [38].

In order to get a better understanding of the role of such surface-surface interactions on the growth and dissolution of surfaces, and the effects of normal stress, we have therefore performed extensive kinetic Monte Carlo (KMC) simulations of a (1+1)-dimensional crystal surface in a confined geometry induced by surface forces. By using KMC we limit the dynamics to transitions between stable states [38], hence there is no need to resolve atomic vibrations explicitly, making simulations on experimental time scales possible. The basic idea is that the crystal surface is in contact with an ideal solution at a constant concentration, and limited by a flat inert surface subject to a constant load. A surface-surface interaction induced in narrow confinement keeps the two surfaces separated. This model is inspired by how confined surfaces in an electrolyte solution repel each other due to the formation of electric double layers [39].

The outline of our model is similar to that of previous models of strained epitaxial and heteroepitaxial growth modeling the ATG instability [40–43]. In these models, a surface subject to the SOS condition not only has a free energy associated with nearest-neighbor bonds, but also a free energy contribution associated with the elastic interactions. Our model of confinement works in a similar manner, except that the elastic interactions are replaced by the surface-surface interaction, the surface diffusion with dissolution, and the calculation of the mechanical equilibrium of springs with the calculation of the mechanical equilibrium of the confining surface. This effectively interchanges the parallel stress with a normal stress, and neglects elastic interactions within the crystal, which we assume are small compared to the surface pressure.

The paper is structured as follows: First we introduce the model, before we compare equilibrium simulations to analytical calculations and thermodynamics. We then investigate how the surface roughness depends on the level of supersaturation, and present a parametrization of the growth and dissolution rates including comparisons with experimental data. We end the paper with discussions and conclusions.

II. MODEL DESCRIPTION

The surface of the crystal at a given time t is described by an array of heights $\mathbf{h}(t)$ with elements $h_i(t) \in \mathcal{Z}$, where $i \in [1, L]$ denotes the surface site. This is equivalent to a two-dimensional lattice with no overhangs, and is referred to as an unrestricted solid-on-solid (SOS) model in $1+1$ dimensions. All position variables are scaled with the lattice unit l_0 representing the physical spacing between two adjacent lattice units. We use periodic boundary conditions, so that $i = 1$ and $i = L$ are considered neighboring sites.

The surface is in contact with an ideal fluid at a constant concentration c of the same particles making up the crystal. Particles can be deposited from the solution to the surface, and dissolved from the surface into the solution. This means that we will not be able to model transport limited scenarios in the current model, but expansion to a general concentration field is possible as long as diffusion within the concentration field is treated properly.

To include the effects of confinement, a flat surface subject to a total force F_0 is placed at a height $h_l(t)$ above the crystal surface. The force is balanced by a repulsive surface-surface interaction given by an ansatz which agrees with DLVO theory for double layer interactions [39] in the limit of two flat surfaces.

Mechanical equilibrium is ensured at all times by repositioning the confining surface [changing $h_l(t)$] such that the net force is zero. An illustration of the system is given in Fig. 1.

In order to properly motivate our ansatz for the surface-surface interaction, we first need to describe how the transitions between surface configurations are modelled, as it puts a localization constraint on the properties of the interaction potential. This will be done in Sec. II A. The ansatz and the localization constraint will be covered in detail in Sec. II B, and the method used to obtain the equilibrium value of $h_l(t)$ will be explained in Sec. II C. In Sec. II D we introduce the simulation parameters, and summarize the simulation steps.

A. State transitions and rates

A state in the model is represented by a unique configuration of heights $\mathbf{h}$ with the confining surface placed at its corresponding equilibrium height h_l. The zero point of the heights is arbitrary, such that a constant shift in all heights (including the confining surface height) will not change the state.

Allowed transitions in the system are deposition and dissolution at all L sites, leading to a unit increase or decrease in the height at this site, respectively. To keep the model as basic as possible, we will not include surface diffusion in any form.

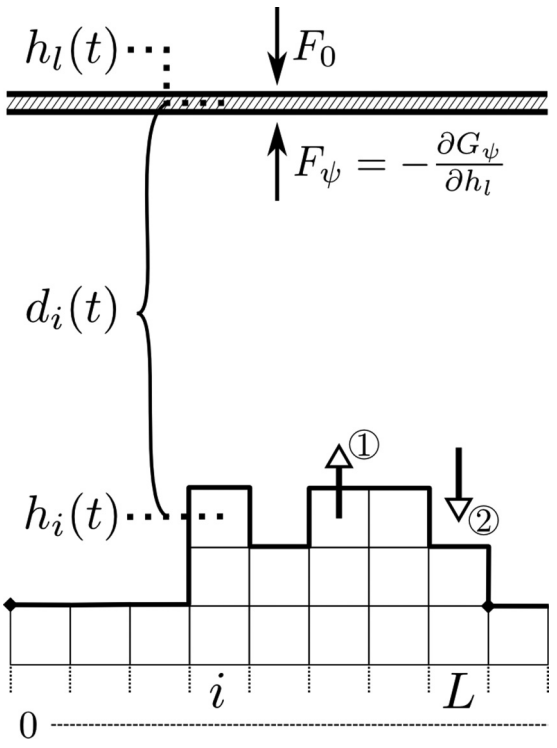

FIG. 1. The confinement model illustrated. A periodic array of L heights $h_i(t)$ makes up the crystal surface. All heights are relative to a fixed arbitrary point (here a zero point below the surface) along the vertical axis. A flat surface, subject to a constant applied force F_0, is located above the crystal surface at a height $h_l(t)$ at which the repulsive surface-surface force F_ψ cancels out F_0 (mechanical equilibrium for all times t). We here skip some function arguments to increase the readability. The free energy G_ψ depends on the surface configuration and h_l, and is generally unknown. In this work we describe this term by an ansatz (introduced in Sec. II B) which depends only on the local separations d_i. The two open arrows denoted by 1 and 2 describe the two types of allowed transitions from a current surface configuration, that is, dissolution and deposition, respectively. Filled arrows represents forces.

This means that we for each such state have $2L$ possible transitions, namely deposition and dissolution at every site. The movement of the confining surface to the new equilibrium height is done instantly after a surface transition has occurred. For large systems, consecutive equilibrium positions are very close in value, so this is believed to be a fair approximation.

In order to couple state transitions to time evolution, we need the transition rates. In this work we use that the rate of a particle moving from its current position at the surface site i (dissolution) is

$$R(i) = \nu \exp\{-[n_i E_b + \Delta G_\psi(i)]/kT\}, \tag{1}$$

where ν is a frequency factor, n_i is the number of nearest neighbors at site i, E_b is the energy of a nearest-neighbor bond, $\Delta G_\psi(i)$ is the surface-surface free energy gained by removing the surface particle at site i from the system, k is the Boltzmann constant, and T is the temperature. This expression is practically identical to the ones used for SOS models of strained epitaxial and heteroepitaxial growth in earlier works, with the exception that the term added to the

nearest-neighbor bond energy represents the change in the surface-surface potential instead of the elastic energy [40–43].

Since the solution is ideal and kept at a constant concentration, there is no change in the free energy when a particle transitions from solution to the surface (deposition). Inserting this into Eq. (1) yields the deposition rate

$$R_+(i) = \nu c, \tag{2}$$

where the concentration c is introduced as the probability of a particle being present around site i (average occupancy), since we do not model particles in the solution explicitly.

It should be mentioned that, in practice, the dissolution and deposition rates should have different frequency factors ν, since these processes are mediated by different physical mechanisms (solution effects and thermal fluctuations). The deposition rate calculated here is a result of using Eq. (1) for the solute transitions as well, which is an approximation used to enable ν to set the time scale for the model. However, if we defined $\tilde{c} \equiv c\nu/\nu_s$, with ν_s being the deposition frequency, we see that the effect of having a separate deposition frequency would simply be to multiply the concentration by the frequency ratio.

We use the rejection free kinetic Monte Carlo (KMC) algorithm [38,44] to evolve the system in time.

B. Confinement free energy ansatz

In the limit of two flat surfaces, we know that the confinement free energy due to the interaction of the electric double layers on each surface is of the form [39]

$$G_\psi^{\text{flat}}(D) = Z_0 \exp(-D/\lambda_D), \tag{3}$$

where D is the surface-surface separation, and λ_D is the Debye length. In this model λ_D and Z_0 are free parameters.

Since our crystal surface is rough, we choose an ansatz of the form

$$G_\psi^{(\text{A})}(\mathbf{h},h_l) = \langle Z_0 \exp(-d_i/\lambda_D)\rangle, \tag{4}$$

where $d_i = h_l - h_i$ is the local separation at site i. This expression agrees with Eq. (3) in the limit where $d_i = D$ for all i (flat surface).

The change in free energy when removing a particle from surface site i, which is what is used in the rate expression in Eq. (1), becomes

$$\begin{aligned}\Delta G_\psi^{(\text{A})}(d_i) &= \frac{Z_0}{L}\exp\left(-\frac{d_i+1}{\lambda_D}\right) - \frac{Z_0}{L}\exp\left(-\frac{d_i}{\lambda_D}\right)\\ &= -\left[1-\exp\left(-\frac{1}{\lambda_D}\right)\right]\frac{Z_0}{L}\exp\left(-\frac{d_i}{\lambda_D}\right).\end{aligned} \tag{5}$$

Note that this change is local, that is, it depends only on the local separation d_i, which is required by Eq. (1).

One could argue that this local ansatz which effectively separates a surface-surface potential into L single particle interactions is not very physical, since a surface-surface interaction generally differs from particle-particle interactions.

A candidate which is not separable is obtained simply by replacing the separation D in Eq. (3) with the average surface-surface separation $\langle d_i\rangle$, that is, $G_\psi^{\text{flat}}(\langle d_i\rangle)$. However, by looking at the change in free energy when removing a particle at site i,

$$\begin{aligned}\Delta G_\psi^{\text{flat}}(i,\mathbf{h}) =& Z_0\exp(-[\langle d_i\rangle + 1/L]/\lambda_D)\\ &- Z_0\exp(-\langle d_i\rangle/\lambda_D)\\ =& -G_\psi^{\text{flat}}(\langle d_i\rangle)\{1-\exp[-1/(L\lambda_D)]\},\end{aligned} \tag{6}$$

it is clear that this expression is not local, since $\langle d_i\rangle$ correlates every height, and consequently it is not of the form of Eq. (1). A nonlinear dependency on $1/L$ is also not ideal. It is therefore clear that the separation of the interaction is necessary to obtain local rates.

Both the nonlocal expression from Eq. (6) and our local expression from Eq. (5) are very crude models of what the exact expression for a rough surface would look like. Effectively, what the local variant does is to ignore higher moments, i.e., neglect $(\langle d_i\rangle^n - \langle d_i^n\rangle)/\lambda_D^n$ for $n \geqslant 2$. In the limit where the roughness of the surface is small (compared to $\langle d_i/\lambda_D\rangle$), which always is the case for the parameters used in this work, these higher moments should also be small, and consequently the difference between these two models should be small as well.

C. Maintaining mechanical equilibrium

The system is said to be in mechanical equilibrium when the magnitude of the repulsive force between the surfaces $F_\psi(\mathbf{h},h_l)$, where h_l is the position of the confining surface, equals the applied force F_0:

$$F_\psi(\mathbf{h},h_l) = F_0. \tag{7}$$

In order to obtain an expression for $F_\psi(\mathbf{h},h_l)$, we calculate the change in the surface-surface free energy $G_\psi(\mathbf{h},h_l)$ as we vary the position of the confining surface h_l:

$$F_\psi(\mathbf{h},h_l) = -\frac{\partial}{\partial h_l}G_\psi(\mathbf{h},h_l). \tag{8}$$

Inserting the derivative of our ansatz from Eq. (4) with respect to h_l into the above equation, the expression for the force becomes

$$F_\psi^{(\text{A})}(\mathbf{h},h_l) = \frac{1}{\lambda_D}G_\psi^{(\text{A})}(\mathbf{h},h_l). \tag{9}$$

The force balance in Eq. (7) now reads

$$\begin{aligned}F_0 &= \frac{Z_0}{\lambda_D}\left\langle \exp\left(-\frac{h_l(t)-h_i(t)}{\lambda_D}\right)\right\rangle\\ &= \frac{Z_0}{\lambda_D}\exp\left(-\frac{h_l(t)}{\lambda_D}\right)\left\langle \exp\left(\frac{h_i(t)}{\lambda_D}\right)\right\rangle,\end{aligned} \tag{10}$$

which when solved for $h_l(t)$ yields

$$h_l(t) = \lambda_D \ln\left(\frac{Z_0\Theta(t)}{\lambda_D F_0}\right), \tag{11}$$

where $\Theta(t) \equiv \langle \exp(h_i(t)/\lambda_D)\rangle$.

This means that when a change occurs at the surface, $\Theta(t)$ will in general change its value, and consequently so will $h_l(t)$. Repositioning of the confining surface must therefore occur every time the surface changes in order to maintain mechanical equilibrium.

In other words, growing the crystal surface will induce a change in the position of the opposing surface. On the other

hand, we should be able to limit growth (or start dissolving) by increasing the confining pressure F_0. These phenomena are commonly referred to as the force of crystallization and pressure solution, respectively [26].

Since the free energy of removing a particle from Eq. (5) depends on the value of $h_l(t)$, and the rates of dissolution from Eq. (1) in turn depend on this free energy, all rates of dissolution change their value once $h_l(t)$ is changed. It is therefore necessary to update these rates to reflect the new value of $h_l(t)$ every time step. An efficient way to update the rates to the new value $h_l(t+\delta t)$ is presented in Appendix A.

D. Simulation parameters and setup

Instead of treating the bond energy E_b and temperature T separately, we define and use

$$\alpha \equiv \frac{E_b}{kT}. \tag{12}$$

This also means that the confining free energy $\Delta G_\psi(i)$ from Eq. (1) will be measured in units of E_b. Introducing the parameter

$$\sigma_0 \equiv \left[1 - \exp\left(-\frac{1}{\lambda_D}\right)\right]\frac{Z_0}{E_b L}, \tag{13}$$

simplifies the expression for $\Delta G_\psi^{(\mathrm{A})}(d_i)$ from Eq. (5):

$$\Delta G_\psi^{(\mathrm{A})}(d_i)/E_b = -\sigma_0 \exp\left(-\frac{d_i}{\lambda_D}\right), \tag{14}$$

where $\sigma_0 \geqslant 0$.

This parameter is easier to use in analyses since it acts as an independent linear factor describing the strength of the surface-surface interaction relative to the binding energy term.

When introducing σ_0, it is convenient to define

$$P_\lambda \equiv \lambda_D \frac{\sigma_0}{Z_0} F_0 = \lambda_D \left[1 - \exp\left(-\frac{1}{\lambda_D}\right)\right]\frac{F_0/E_b}{L}, \tag{15}$$

as a measure proportional to the applied pressure F_0/L, such that Eq. (11) now reads

$$h_l(t) = \lambda_D \ln\left(\frac{\sigma_0 \Theta(t)}{P_\lambda}\right). \tag{16}$$

In order to better understand the role of σ_0, we can use the average surface-surface separation $\langle d_i \rangle = h_l - \langle h_i \rangle$ to write

$$\sigma_0 = P_\lambda \xi(\mathbf{h}) \exp\frac{\langle d_i \rangle}{\lambda_D}, \tag{17}$$

where

$$\xi(\mathbf{h}) = 1 + \left(\frac{\sigma(\mathbf{h})}{\lambda_D}\right)^2 + \mathcal{O}\left(\frac{\langle (h_i - \langle h_i \rangle)^4 \rangle}{\lambda_D^4}\right), \tag{18}$$

is typically close to 1 with

$$\sigma(\mathbf{h})^2 = \frac{1}{L}\sum_{i=1}^{L}(h_i - \langle h_i \rangle)^2, \tag{19}$$

being a measure of the surface roughness. In practice we find that the change in $\sigma(\mathbf{h})^2$ due to a change in σ_0 is small compared to the corresponding change in $\langle d_i \rangle$. This means that we can interpret σ_0 as the parameter controlling the average surface-surface separation for a given pressure P_λ and decay length λ_D.

We also define and use

$$\gamma \equiv \ln\frac{c}{c_0}, \tag{20}$$

instead of using the concentration c directly, where $c_0 = \exp(-2\alpha)$ is the equilibrium concentration for the unconfined system [45].

The saturation level $\Omega \equiv c/c_{\mathrm{eq}} - 1$, where c_{eq} is the equilibrium concentration of the confined system, is the main driving force for crystal growth (supersaturated $\Omega > 0$) and dissolution (undersaturated $\Omega < 0$). By rewriting the expression for γ from Eq. (20) as

$$\gamma = \ln\left(\frac{c}{c_{\mathrm{eq}}}\frac{c_{\mathrm{eq}}}{c_0}\right) = \ln(1+\Omega) + \gamma_{\mathrm{eq}}, \tag{21}$$

where $\gamma_{\mathrm{eq}} \equiv \ln c_{\mathrm{eq}}/c_0$ is the value of γ in equilibrium, we see that the saturation level can be controlled directly if we first obtain γ_{eq}. Equilibration is thus an essential first step to all simulations, even if we are to simulate out of equilibrium (see Appendix B).

Once the value of γ_{eq} is obtained, we shift the value of γ by $\ln(1+\Omega)$, where Ω is the sought saturation level, and start the main simulation.

The single simulation for a given value of γ can be summarized in the following steps:

(1) Input γ, α, P_λ, λ_D, σ_0, and set $\mathbf{h}(0)$.
(2) Calculate $h_l(0)$ by Eq. (16).
(3) Calculate all rates (dissolution and deposition).
(4) Use KMC to select and perform a transition.
(5) Calculate new value of $h_l(t)$.
(6) Sample values for averages.
(7) If not done, update rates and go to step (5).
(8) Finalize averages.

A complete simulation at a given level of supersaturation Ω can be summarized in the following steps:

(1) Input α, P_λ, λ_D, σ_0, and set $\mathbf{h}(0)$.
(2) Calculate γ_{eq} (see Appendix B).
(3) Set $\gamma = \gamma_{\mathrm{eq}} + \ln(1+\Omega)$ and do the simulation steps.

Since the average time step in KMC is proportional to $1/L$, an unnecessarily large system should be avoided. In order to select an appropriate system size L, we calculated the value of system size independent quantities such as the surface roughness and energy density for simulations with $L = 64, 128, 256, 512$, and $L = 1024$. We found that, in practice, the boundary effects are negligible at $L = 128$, where the results are indistinguishable from the $L = 1024$ case. However, in order to be sure that the simulations do not suffer from boundary effects we have chosen to use $L = 256$ in this work.

III. RESULTS

From the force balance criteria in Eq. (10) it is clear that increasing the pressure will decrease the average surface-surface separation $\langle d_i \rangle$ in roughly a exponentially decaying manner. The assumption that $\langle d_i \rangle/\lambda_D$ is small introduced in Sec. II B, thus translates into an upper limit to the pressure

P_λ for a given σ_0 and λ_D. For $\sigma_0 = 1$ and $\lambda_D = 4$, we get an average surface separation of $\langle d_i \rangle = 3$ when $P_\lambda = 0.5$. We therefore use values of $P_\lambda \in [0,0.5)$. In some plots, a value of $P_\lambda = 1$ is used to make the high pressure limit very prominent.

Due to large surface fluctuations and slow convergence to steady state, satisfactory measurements become increasingly demanding to produce as α becomes smaller. Hence we have chosen to study $\alpha \in [0.5,3]$, where $\alpha = 0.5$ produces rough surfaces with large steps and $\sigma(\mathbf{h}) \sim 17$, and $\alpha = 3$ produces flat surfaces with typical step sizes of 1 or 2. The limit where $\alpha \to 0$ is studied for equilibrium simulations.

A. Equilibrium simulations

1. Thermodynamical validations in the unconfined limit

Since the joining of two particles without confinement increases the total free energy by E_b, each available site along the surface, both vertically and horizontally, carries a potential energy of $E_b/2$. It is therefore convenient to write the Hamiltonian of the unconfined system as $H(s) = E_b s/2$, where s is a count of the number of surface sites exposed to the solution.

Because of the periodic boundary conditions and the no overhang criteria, we may write $s = 2s_{\uparrow\downarrow} + L$, where $s_{\uparrow\downarrow}$ is the total number of upward steps, which necessarily have to equal the corresponding downward value, hence the use of both arrows. Since E_b and L are system constants, we can simplify the Hamiltonian to $\tilde{H}(s_{\uparrow\downarrow}) = E_b s_{\uparrow\downarrow}$, by introducing an energy shift of $E_b L/2$. This yields the following partition function:

$$Z(L,\alpha) = \sum_{s_{\uparrow\downarrow}=0}^{\infty} M_{\text{tot}}(s_{\uparrow\downarrow},L)\exp(-\alpha s_{\uparrow\downarrow}), \tag{22}$$

where $M_{\text{tot}}(s_{\uparrow\downarrow},L)$ is the multiplicity of surfaces with the given value of $s_{\uparrow\downarrow}$. The calculation of the multiplicity is given in Appendix C. At which value of $s_{\uparrow\downarrow}$ the sum can be truncated without loss of numerical precision depends on the value of α, but we found $s \simeq 20\,000$ to be sufficient for the results presented here.

From the partition function we can calculate thermodynamic variables in the canonical ensemble as follows:

$$\langle E \rangle / E_b = \langle s_{\uparrow\downarrow} \rangle, \tag{23}$$

$$\sigma(E)/E_b = \sigma(s_{\uparrow\downarrow}) = \sqrt{\langle s_{\uparrow\downarrow}^2 \rangle - \langle s_{\uparrow\downarrow} \rangle^2}, \tag{24}$$

$$C_V/k = \alpha^2 \sigma(s_{\uparrow\downarrow})^2, \tag{25}$$

where $\sigma(s_{\uparrow\downarrow})$ is the square root of the vertical surface size variance, E is the energy, $\sigma(E)$ is the square root of the energy variance, and C_V is the specific heat capacity.

By using Eq. (22) we can calculate all these quantities by evaluating closed form expressions.

When we add the confining surface, these thermodynamic relations are no longer valid. This is because the free energy of the system no longer is given in terms of the surface size s alone.

However, regardless of their thermodynamical interpretation, the right-hand side of Eqs. (23)–(25) can be estimated numerically and compared to the unconfined system. This also allows us to validate the model by ensuring convergence to closed form solutions in the unconfined limit. The results of these simulations are given in Fig. 2, where it is clear that the model indeed converges to the known solutions in the zero applied force limit. Moreover, we observe that an increase in the applied force flattens the surface and suppresses surface fluctuations.

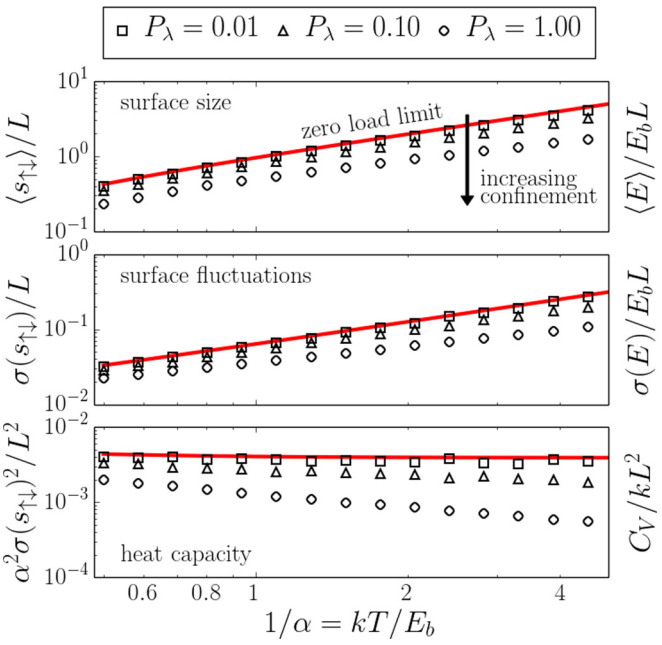

FIG. 2. Simulations done in equilibrium for a system with size $L = 256$ for different values of $P_\lambda \propto F_0/L$, where F_0/L is the applied pressure. For these simulations, we used $\sigma_0 = 1$ and $\lambda_D = 2$. The solid lines represent the closed form solutions to the unconfined system. The statistical errors are increasing with $1/\alpha$, but overall small enough to not impact the trends shown here. The left axis label represents the calculated quantity, and for $P_\lambda \to 0$ (no confinement), the right axis label represents the respective thermodynamic quantity. From the top and middle panels we see that for low pressures, the average vertical crystal surface size $\langle s_{\uparrow\downarrow} \rangle$ and its fluctuation appear linear in the logarithmic scale of $1/\alpha$ with slopes close to 1, indicating that they are proportional to $1/\alpha$. This ultimately results in a constant heat capacity C_V/k in the limit of no confinement, seen in the bottom panel. It is clear from these results that the effects of increasing the pressure F_0/L is to flatten the surface and dampen the surface fluctuations.

2. Thermodynamical validations with confinement

Growing a layer of thickness d_N consisting of N particles under a constant force F_0 carries a free energy cost of $G_N = F_0 d_N - 2E_b N$, where the last term comes from the fact that on average, each deposition creates two new bonds of energy E_b. This translates into a solid chemical potential of $\Delta\mu_s = G_N/N = F_0/L - 2E_b$. In equilibrium, this equals the solution chemical potential given by $kT \ln c_{\text{eq}}$, which yields

$$\begin{aligned} F_0/L &= kT \ln c_{\text{eq}} + 2E_b, \\ &= kT \ln(c_{\text{eq}}/c_0), \end{aligned} \tag{26}$$

where we used that the unconfined equilibrium concentration $c_0 = \exp(-2E_b/kT)$. This identity is equal to that derived

in Refs. [25,27,46] for a surface consisting of monoatomic particles growing under a constant "crystallization pressure" (here given by F_0/L).

Introducing the parameters $\alpha = E_b/kT$ and $\gamma_{\text{eq}} = \ln(c_{\text{eq}}/c_0)$, we get

$$\frac{F_0/E_b}{L} = \frac{\gamma_{\text{eq}}}{\alpha}. \tag{27}$$

In our simulations we use P_λ from Eq. (15) instead of $(F_0/E_b)/L$. To convert between these two is a matter of multiplying by a single factor which depends on the decay length λ_D of the surface-surface interaction. In terms of the simulation parameters, Eq. (27) reads

$$\frac{\alpha P_\lambda}{\gamma_{\text{eq}}} = \lambda_D\left[1 - \exp\left(-\frac{1}{\lambda_D}\right)\right]. \tag{28}$$

We can in other words compare our model with basic thermodynamics in confinement by checking if the parameters of our model are related by Eq. (28).

This is done in a three-step process which is presented in Fig. 3. From Fig. 3(a) we see that there is a linear relationship between γ_{eq} and α. We can thus measure $\gamma_{\text{eq}}/\alpha$ as the slope of these lines. This is done in Fig. 3(b), where we find that there is a linear dependence between the measured value of $\gamma_{\text{eq}}/\alpha$ and P_λ. The second step then naturally involves measuring the slope of this line as $\gamma_{\text{eq}}/\alpha P_\lambda$. Finally, we compare the inverse of this measurement to the right-hand side of Eq. (28). This is shown in Fig. 3(c). The relationship in Eq. (28) was found to hold for all choices of σ_0 (17 values of $\sigma_0 \in [0.1,5)$ were checked).

From the figure, we see that there is a very good match for $\lambda_D > 0.5$, which means that our model for confinement agrees well with the thermodynamics in Eq. (28) for a reasonable choice of parameters.

The discrepancy for low values of λ_D is believed to be present partially due to low sampling ergodicity for low λ_D. Moreover, the movement of the confining surface is very violent in the sense that the distance at which it is moved becomes very large. Therefore, we violate the assumption that this movement is small.

Additionally, in KMC we do not necessarily increase the surface height by growing single layers at the time (as is assumed in the analytical derivation). In the extreme limits of the parameters, such that $\lambda_D < 0.5$, it makes sense for the consequence of this difference to become more prominent.

In other words, the model obeys the thermodynamical relation in Eq. (27) very well for all reasonable choices of parameters.

B. Out-of-equilibrium simulations

1. *Steady state convergence and roughness calculations*

In steady state, we expect measured quantities to converge to and fluctuate around characteristic values which, in general, will depend on the saturation level. An example of convergence to steady state is given in Fig. 4, where we clearly see the calculated quantities, such as the surface roughness, reaching a plateau value after a given time.

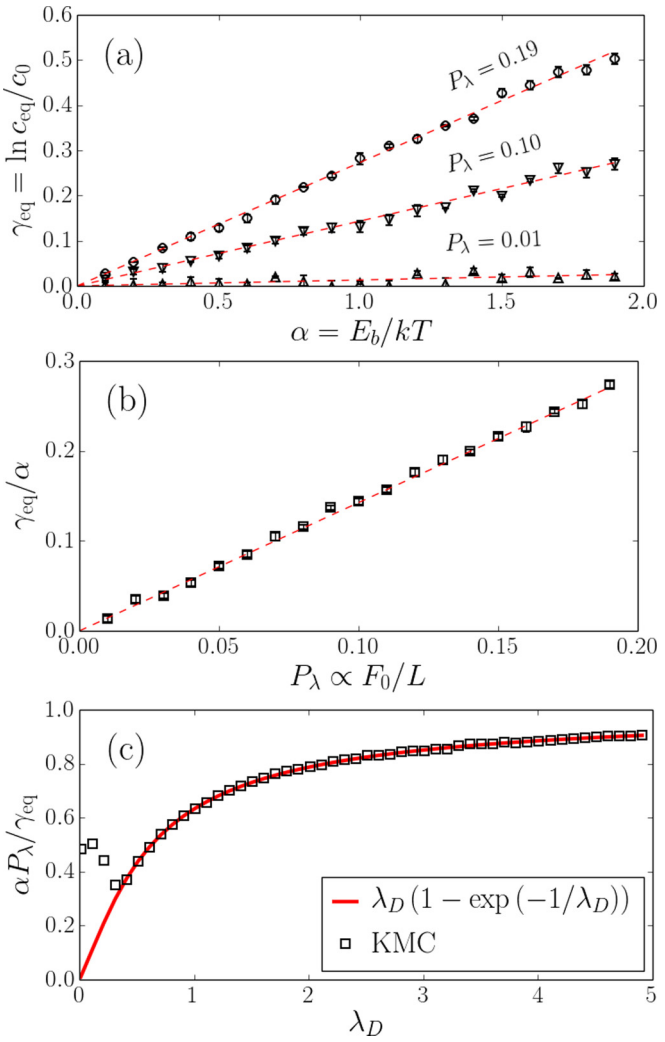

FIG. 3. Results of parametrization of the thermodynamic relation from Eqs. (27) and (28). In (a) and (b) we used $\sigma_0 = 1.0$ and $\lambda_D = 1.61$. The dashed lines represent the result of the linear fitting of the data, whose slope are used to estimate the ratio between the quantities along the vertical and horizontal axes. In (c), the result of averaging the ratio of the axes in (b) for several $\sigma_0 \in [0.1,5)$ is shown together with the analytical solution given by Eq. (28). We observe a good fit for $\lambda_D > 0.5$, indicating that the model reproduce basic thermodynamics very well. A total of $\sim 3 \times 10^5$ equilibration simulations were done to generate the bottom plot.

The surface roughness is a standard measure of the surface geometry, and is a commonly measured quantity in experiments [47].

In Fig. 5 we see how the surface roughness depends on the saturation level and confinement pressure for different values of α. As expected from Fig. 2, the overall roughness decrease with increasing α and confinement pressure. The overall trend for growth ($\Omega > 0$) is that the roughness increases as we increase the supersaturation. This can be explained by the fact that as the random deposition becomes more and more dominant, the ability of the geometry dependent dissolution reactions to dissolve particles deposited at unfavorable locations is suppressed.

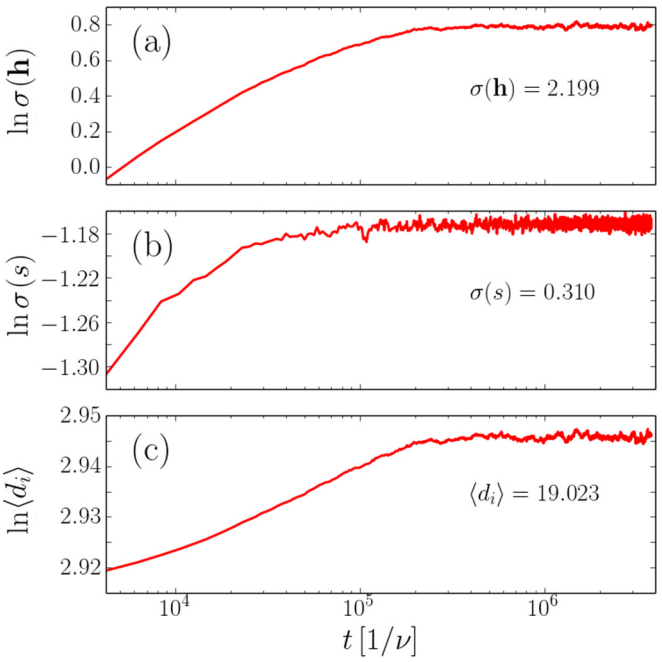

FIG. 4. Steady state convergence of the $\sigma(\mathbf{h})$ from Eq. (19), the square root of the temporal surface length variance $\sigma(s)$, and the average distance between the crystal and the confining surface $\langle d_i\rangle$. The time unit of $1/\nu$ comes from the rate expression in Eq. (1). The smooth nature of the graphs are a result of combining 1000 simulations of the same system. For these simulations we used $L = 256$, $\Omega = -3/4$, $\alpha = E_b/kT = 3.0$, $P_\lambda = 0.01$, $\lambda_D = 4.0$, and $\sigma_0 = 1.0$. We clearly see that the values converge to a plateau value, which is what we refer to as the steady state value. The steady state value of the calculated quantities are placed in the plots.

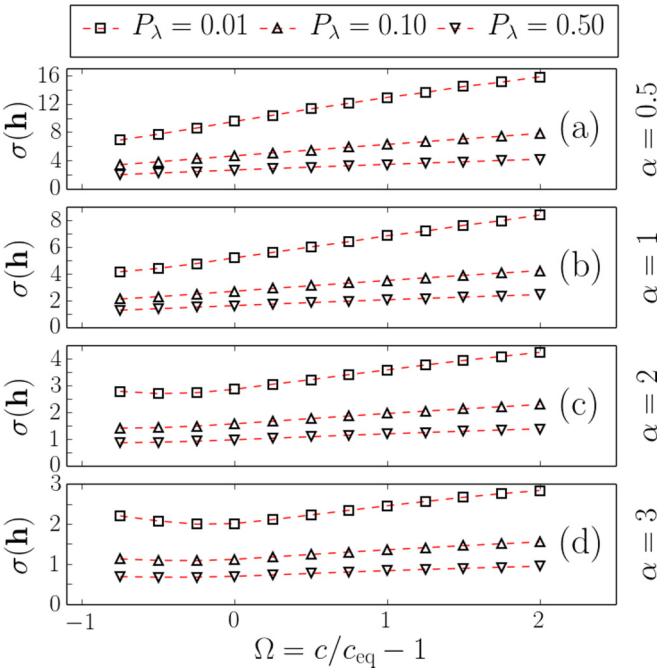

FIG. 5. Steady state surface roughness $\sigma(\mathbf{h})$ from Eq. (19) as a function of the saturation level Ω for different values of $\alpha = E_b/kT$. The simulations were performed using $L = 256$, $P_\lambda = 0.01$, $\lambda_D = 4.0$, and $\sigma_0 = 1.0$. We see that as we increase α, the overall magnitude of the surface roughness is decreasing. For growth ($\Omega > 0$), the roughness tends to increase with supersaturation. For dissolution ($\Omega < 0$), we can either have a decrease or an increase in the roughness by increasing Ω, depending on the value of α.

This trend extends to dissolution ($\Omega < 0$) only for low values of α. In the case for high values of α, further lowering the saturation level for dissolving systems has the same effect as further increasing the supersaturation had for growth, and we approach a system that is symmetric around equilibrium ($\Omega = 0$) with respect to the saturation level.

One might suggest that this sudden increase in roughness for dissolving systems arise due to sampling errors and bad convergence, however, looking at Fig. 4(a), which represents the lowest supersaturation for the highest α in Fig. 5(d), we clearly see that this is not the case.

These results are in perfect agreement with experiments, where it is reported that an increasing supersaturation leads to an increasing surface roughness, whereas a low supersaturation will increase the roughness only for high surface energy crystals (high α) [47].

An explanation for this phenomenon could be that as we approach high values of α, the surface roughness becomes so small that the free energy cost of creating an even flatter surface becomes dominated by the large decrease in entropy in this flat limit. In other words, as the surface becomes very flat, kink sites are still more energetically favorable to remove than a flat site, however, due to the large number of flat sites as compared to kink sites, dissolving a flat site, and thus increasing the roughness, will become more likely.

2. *Calculating the linear growth rate constant*

Another commonly measured quantity in experiments is the linear growth speed $\dot{H} = \delta\langle h\rangle/\delta t$ as the change in size (height or mass) over a given time period δt [48–54].

In these experiments, the linear growth (or dissolution) speed $\dot{H}$ is typically found to be related to the saturation level Ω as follows:

$$\dot{H} = k_g \Omega^n, \tag{29}$$

where k_g is a proportionality constant referred to as the linear growth rate constant, and the exponent n is measured to be in the range between 1 and 2 [48]. It is suggested that $n = 1$ far from equilibrium, and $n = 2$ close to equilibrium [49,50].

Using Eq. (29), we may interpret k_g as the ability of the system to respond to changes in the saturation level. For high k_g, a small change in the saturation level will result in a large change in the growth velocity, whereas the opposite is true for low k_g. The linear growth rate constant k_g generally depends on all the state parameters of the system. By studying the growth rate constant, we can in other words gain insight into how different state parameters influence how the system responds to changes in the saturation level.

In order to study k_g, we measured the growth speed for saturations levels $\Omega \in (-1,2]$ for various combinations of parameters using $\lambda_D \in [1,5]$ and $\sigma_0 \in [0.1,2]$.

By looking closely at Fig. 6(a), we see that there are separate linear trends for $\Omega > 0$ and $\Omega < 0$ with different

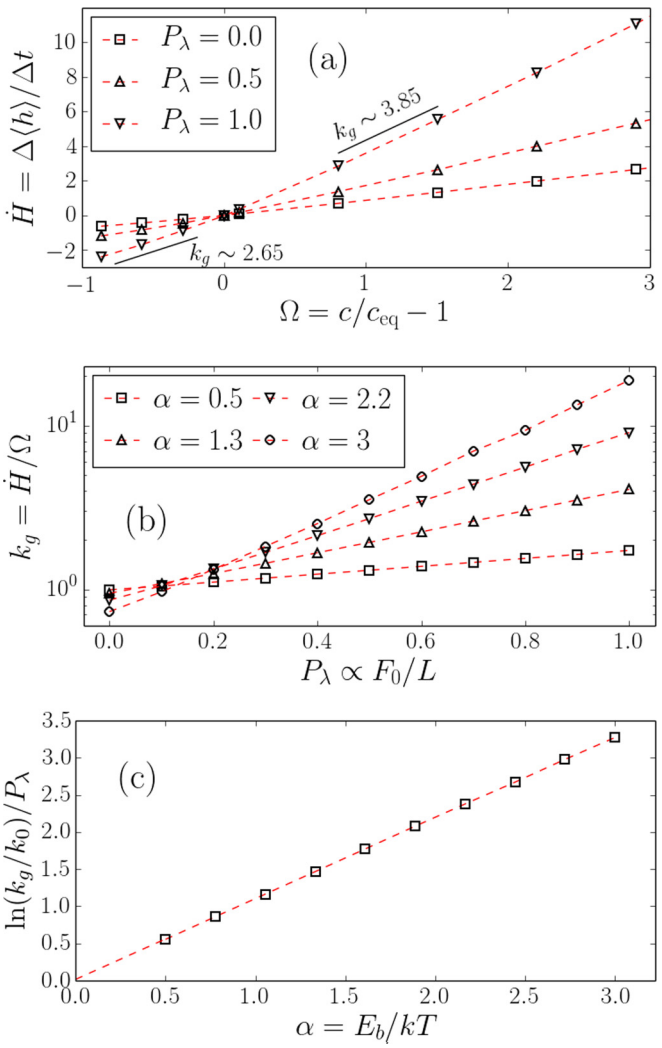

FIG. 6. Results showing the linear growth rate $\dot{H}$ vs the saturation level $\Omega = c/c_{\rm eq} - 1$. Analyses of (a) indicate the existence of two separate linear relationships for growth ($\Omega > 0$) and dissolution ($\Omega < 0$). The slope represents the linear growth rate constant k_g. Without confinement ($P_\lambda = 0$), the trends presented here are identical to those found for $\alpha < 0.75$ in Ref. [56]. In (b), the results of the dependency of k_g on α and P_λ are shown for $\Omega > 0$. The plot suggests the existence of a common point P' along the P_λ axis where $\ln k_g$ is independent of α, and a linear dependency of α outside this. This point has been estimated to be 0.14 for growth and 0.53 for dissolution. For values of $\alpha < 1$, the corresponding lines start to deviate from this common point in a nontrivial manner. The slopes of the lines from (b) vs α are shown in (c). This shows the slope to be very close to α, indicating that $\ln k_g \sim \alpha(P_\lambda - P')$. This is general for all values of σ_0 and for $\lambda_D > 2$. These simulations were performed using $L = 256$, $\sigma_0 = 1.05$ and $\lambda_D = 7/3$. In (a), we used $\alpha = 4/3$.

slopes (different k_g). This effect is more prominent the higher the confining pressure P_λ is.

This asymmetry is in agreement with observations made in crystal growth and dissolution experiments [51,52], as well as earlier work using the basic model without confinement [55].

The transition between two linear regimes around $\Omega = 0$ also agrees with the fact that exponents $n > 1$ in Eq. (29) are observed close to equilibrium [49,50].

Looking at Fig. 6(b), we find that there is a linear relationship between $\ln(k_g)$ and P_λ, starting from the unconfined solution $\ln k_0$ in $P_\lambda = 0$. It seems like the lines for all α intersect at a common point. These trends were present for both growth and dissolution, and the common intersections were found at $P_\lambda \simeq 0.14$ and $P_\lambda \simeq 0.53$, respectively. The location of the point was found to be independent of σ_0 and λ_D, however, for $\alpha < 1.0$ the lines start shifting away from the common intersection in a nontrivial manner. An explanation to this behavior could be that the assumption that the roughness is small compared to the average surface-surface separation is violated.

Figure 6(c) shows $\ln(k_g/k_0)/P_\lambda$ as a function of α, and reveals yet again a linear relationship, this time going through the origin with a slope very close to 1. The final parametrization reads

$$\ln k_g/\nu \simeq \begin{cases} \alpha(P_\lambda - 0.14), & \Omega > 0, \lambda_D \geqslant 2, \alpha > 1 \\ \alpha(P_\lambda - 0.53), & \Omega < 0, \lambda_D \geqslant 3, \alpha > 1 \end{cases}. \quad (30)$$

The exponential dependency on $\alpha \propto 1/T$ is in agreement with experiments [49,53,54] and earlier work on the unconfined system for $\alpha < 0.75$ without separate analyses of growth and dissolution [56].

The linear trends which our analysis relies on are present for all values of σ_0, but breaks down for $\lambda_D < 3$ for dissolution and $\lambda_D < 2$ for growth. It seems feasible that the cause of this breakdown is similar to the cause of the discrepancy between the thermodynamics and the model for low λ_D in Fig. 3(c).

A problem with lattice KMC is that we do not know the proper time unit, as we use an idealized rate expression which does not involve calculating the activation energy barrier. The growth rate is therefore not directly comparable to experiments. However, if we look at the ratio between the linear growth rate constant for growth and dissolution, we find

$$\ln(k_g^+/k_g^-) \simeq 0.39\alpha, \quad (31)$$

which should to a certain degree cancel out the unknown time scale, making Eq. (31) a potential candidate for comparison with experiments. More specifically, it would be interesting to see if the ratio in Eq. (31) would depend on the applied force or not in an experimental environment.

These results indicate that the effect of confinement on the rate constant is independent of whether the system is growing or dissolving. This means that the asymmetry between growth and dissolution is neither a result of, nor enhanced by, the pressure. It is hard to compare our results directly to the earlier work done without confinement in $2+1$ dimensions for $\alpha < 0.75$ in Ref. [56], since our parametrization does not extend into this high-temperature range. What is in agreement, however, is that the rate of growth is higher than that of dissolution, with a difference which decreases with higher α.

IV. DISCUSSIONS AND CONCLUSIONS

The aim of this work was to study the effect of normal stress on a $(1+1)$-dimensional unrestricted solid-on-solid (SOS) surface generated by a surface-surface interaction with a confining flat surface. We achieved this by including a local

energy which agreed with DLVO theory in the limit of two flat surfaces.

The model produces phenomena like the force of crystallization and pressure solution simply due to an interplay between a chemical instability in the form of a supersaturation and a mechanical instability in the form of a balance between an external confining force F_0 and the generated repulsive force. This demonstrated that the model, despite its simplicity, is able to produce nontrivial physics. This in turn enables us to study nontrivial processes in terms of simple parameters, such as the supersaturation.

Replacing the exponential ansatz for the surface-surface repulsion by another monotonically decreasing function should produce the same overall behavior, since the important property of this interaction is that there exists one unique equilibrium point for any given surface configuration, and that an increased confinement produces an increased repulsion. Nevertheless, using an expression which is derived from DLVO theory enables us to see the interaction parameters in light of existing theories, which makes the results easier to interpret.

The equilibrium concentration as a function of applied external pressure was found to be independent of the interaction parameters for $\lambda_D > 0.5$ and agreed perfectly with known thermodynamics. We also found a smooth transition to thermodynamics calculated without confinement as we let the confining force tend to zero. This demonstrates that the model produces the correct macroscopic limit, that the microscopic equilibrium is well defined, and that the state parameters used (force, pressure, temperature, etc.) are comparable to macroscopic quantities.

A strength of the model is that all the parameters can be easily linked to well-defined physical quantities such as saturation level, applied force, Debye length, temperature, surface tension, average surface-surface separation, etc., which makes it easy to relate to physical systems, and then in turn easy to analyze.

Limitations of the model, besides those of the SOS model, are the simple description of the solution and the limitation to moderate pressures. Since we do not calculate energy barriers, we do not possess information about the real time scale, which renders it difficult to properly measure dynamic variables such as, e.g., the surface speed, as well as to measure anything outside steady state in a manner which is comparable to other models or experiments.

The fact that we can produce highly nontrivial processes with such a high level of agreement with the macroscopic limit makes the model very convincing. We therefore believe that the model accomplishes very well what it is designed to do, that is, model the effect of normal stress on a confined surface. Hence we believe this work will aid with understanding the behavior of crystals in highly confined media such as nanoporous structures, microfractures, etc., which are systems with important practical applications.

Due to the extreme finite-size effects limiting the motion of ions in solution, transport is a crucial limiting factor in confined systems. Hence if we want to properly model highly saturated systems, we need a model of the solution which takes into account the transport of material from a bulk reservoir into the cavity and to the surface. Simply expanding the crystal lattice into solution would not be optimal as this dramatically underestimates the degrees of freedom in solution, which is crucial to include in their completeness due to the confining nature of the system. Coupling a time integration type of free diffusion model to the current master equation is part of our ongoing work, and when successful, it will allow us to model environments in which the confined system is coupled to a reservoir in a more physically correct manner. An example of a process in such an environment is the rim formation on confined growing crystals surrounded by a supersaturated solution [23,24,32], which would be the extension of the model presented in this work to three dimensions.

ACKNOWLEDGMENTS

Discussions with O. P. Luois significantly contributed to this paper. This study was supported by the Research Council of Norway through the project "Nanoconfined crystal growth and dissolution" (No. 222386). We acknowledge support from the Norwegian High Performance Computing (NOTUR) network through the grant of machine access.

APPENDIX A: EFFICIENTLY UPDATING DISSOLUTION RATES

Since we use absolute heights, using the value of $\Theta(t)$ in Eq. (16) directly will lead to floating point errors. This is circumvented by using the change in the equilibrium height of the confining surface $h_l(t)$ between two steps instead of explicitly recalculating it every step:

$$\begin{aligned}\delta h_l(t+\delta t) &= h_l(t+\delta t) - h_l(t) \\ &= \lambda_D \ln\left(\frac{\Theta(t+\delta t)}{\Theta(t)}\right),\end{aligned} \tag{A1}$$

because the ratio of two consequent $\Theta(t)$ will be close to 1.

The ratio is calculated as

$$\frac{\Theta(t+\delta t)}{\Theta(t)} = \sum_{i=1}^{L} \exp\{[h_i(t+\delta t) - \lambda_D \ln\Theta(t)]/\lambda_D\}, \tag{A2}$$

which, when inserting Eqs. (14) and (16) yields

$$\frac{\Theta(t+\delta t)}{\Theta(t)} = \frac{1}{P_\lambda}\sum_{i=1}^{L} \Delta G_a[h_l(t) - h_i(t+\delta t)]/E_b. \tag{A3}$$

Since every dissolution rate depends on $h_l(t)$, these need to be updated for all sites after every step, which is very expensive compared to the rest of the simulation. However, we can optimize these calculations by using that every site except three preserves its number of neighbors n_i and their heights h_i every step. The only change in their rates comes from the fact that the load height changes from $h_l(t)$ to $h_l(t+\delta t) = h_l(t) + \delta h_l(t)$.

Defining $G_i(t) \equiv \Delta G_\psi^{(\mathrm{A})}(\delta h_i(t))$ and $R_i \equiv \hat{R}_-(i)$, we can rewrite these unaffected dissolution rates for the next time step as

$$\begin{aligned}R_i(t+\delta t) &= R_i(t)\frac{R_i(t+\delta t)}{R_i(t)} \\ &= R_i(t)\exp\big(-\alpha[G_i(t+\delta t) - G_i(t)]\big) \\ &\equiv R_i(t)\exp\big(-\alpha\delta G_i(t)\big),\end{aligned} \tag{A4}$$

where

$$\delta G_i(t) = G_i(t)\left(\frac{G_i(t+\delta t)}{G_i(t)} - 1\right)$$
$$= G_i(t)\left[\exp\left(-\frac{\delta h_l(t)}{\lambda_D}\right) - 1\right]. \quad \text{(A5)}$$

These expressions involve evaluating the exponential function of a very small number, which can be approximated by a (preferably odd leading powered) series expansion $T(x) \simeq \exp(x)$ around $x = 0$.

This leads us to the following algorithm for updating the load height and rates:

(1) Calculate $\delta h_l(t)$ from Eq. (A1).
(2) Set $h_l(t+\delta t) = h_l(t) + \delta h_l(t)$.
(3) Calculate $\kappa(t) \equiv T(-\delta h_l(t)/\lambda_D)$.
(4) Update $R_i \to R_i \times T(-\alpha G_i(t)[\kappa(t) - 1])$, unless the number of neighbors or height at site i changed the previous time step, then do a full recalculation.
(5) Update $G_i \to G_i \times \kappa(t)$, unless the height at site i changed the previous time step, then recalculate.

APPENDIX B: EQUILIBRATION

The equilibrium condition written in terms of rates is

$$\langle R_- \rangle_{t,L} = \langle R_+ \rangle_{t,L}, \quad \text{(B1)}$$

where $\langle\rangle_{t,L}$ denotes an average in both time and space, and R_- and R_+ are the rates of dissolution and deposition, respectively.

Inserting the expressions for the dissolution and deposition from Eqs. (1) and (2) yields

$$\left\langle \exp\{-\alpha[n_i - 2 + \Delta G_\psi(i)/E_b] - \gamma_{\rm eq}\}\right\rangle_{t,L} = 1, \quad \text{(B2)}$$

where $\gamma_{\rm eq}$ is the equilibrium value of γ, defined in Eq. (20).

At first glance it may seem like the solution is trivial since $\gamma_{\rm eq}$ can be taken outside the averages and be isolated, however, since the average itself generally depends on the concentration (through the number of neighbors, etc.), this leads to a self-consistent equation.

Instead, assume that we are simulating at some given $\gamma_k = \gamma_{\rm eq} + \delta\gamma_k$, where $\delta\gamma_k$ is the shift necessary to bring the system to equilibrium. Then inserting $\gamma_{\rm eq} = \gamma_k - \delta\gamma_k$ in Eq. (B2) and isolating $\delta\gamma_k$ gives us

$$\delta\gamma_k = \ln\langle R_-/R_+\rangle_{t,L}, \quad \text{(B3)}$$

where the time average is done with $\gamma = \gamma_k$. If we now update the value of γ according to the recurrence relation

$$\gamma_{k+1} = \gamma_k + \delta\gamma_k, \quad \text{(B4)}$$

we expect to converge to the equilibrium value of γ in the following manner:

$$\lim_{k\to\infty} \gamma_k = \gamma_{\rm eq}. \quad \text{(B5)}$$

This is equivalent to solving Eq. (B2) by fix point iteration.

In practice, because of statistical fluctuations in the calculation of the new step $\delta\gamma_k$, we stop after N iterations and do an averaging over all the calculated γ_k from the point $k = k_0$ where the shift first changed sign:

$$\gamma_{\rm eq} \simeq \frac{1}{N - k_0}\sum_{k=k_0}^{N} \gamma_k. \quad \text{(B6)}$$

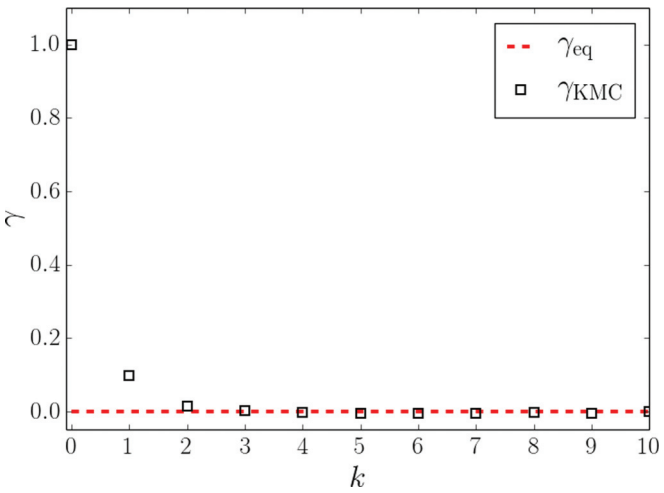

FIG. 7. The ten first iterations of γ_k (squares) with iteration steps k for a $L = 256$ and $\alpha = 1$ basic model without confinement. For this run we used 10^4 cycles per iteration and $N = 100$ total iterations. In practice, a good enough estimate is obtained after around ten iterations, however, in order to get a fair estimate of the spread, additional iterations are performed. The initial value is $\gamma_0 = 1$, and the exact solution is $\gamma_{\rm eq} = 0$. The final result gave $\gamma_{\rm eq} = 0.00(6)$.

An estimate of the error is obtained by calculating the standard deviation of the γ_k used to estimate $\gamma_{\rm eq}$. A more intuitive method would be to stop when the shift has reached some threshold value, however, this is not very practical due to statistical fluctuations.

Figure 7 shows the iteration to equilibrium for an unconfined system starting away from equilibrium, and ending up very close to the exact solution of $\gamma_{\rm eq} = 0$.

APPENDIX C: ANALYTICAL CALCULATIONS

We want to calculate the number of ways we can construct a surface of size s on a system of size $L \geqslant 3$.

The surface size s can be decoupled into three parts as follows:

$$s = s_\uparrow + s_\downarrow + s_\rightarrow, \quad \text{(C1)}$$

where the arrows indicate the direction of the surface.

Since we do not allow overhangs, we must have that $s_\rightarrow = L$. Moreover, since we use periodic boundary conditions, we must go equal parts up and down to arrive back where we started. In other words, we have that $s_\uparrow = s_\downarrow \equiv s_{\uparrow\downarrow}$, which yields $s = 2s_{\uparrow\downarrow} + L$.

We can group configurations by the number of sites that contains $n_\uparrow$ number of steps up, $n_\downarrow$ number of steps down and $n_\rightarrow$ number of flat steps (neighbors of equal height). Using the restrictions $n_\uparrow + n_\downarrow + n_\rightarrow = L$, that is, a step has to be either up, down, or flat, we can effectively reduce the degrees of freedom by one by imposing $n_\rightarrow = L - n_\uparrow - n_\downarrow$.

For a given set of $n_\downarrow$ and $n_\uparrow$, the number of ways to combine these on L sites is

$$M_n(\mathbf{n}) = \frac{L!}{n_\uparrow!\, n_\downarrow!\, n_\rightarrow!}, \tag{C2}$$

where $\mathbf{n}$ represents $n_\downarrow$, $n_\uparrow$, and $n_\rightarrow$.

From here we need to know the number of ways to distribute a given value of $s_{\uparrow\downarrow}$ among $n_\downarrow$ and $n_\uparrow$. We have that each site must contain at least one step up or down, hence $n_\uparrow$ and $n_\downarrow$ must be less than or equal to $s_{\uparrow\downarrow}$.

Let n denote either $n_\uparrow$ or $n_\downarrow$, then the number of ways to do this is

$$m(n,s_{\uparrow\downarrow}) = \frac{(s_{\uparrow\downarrow}-1)!}{(s_{\uparrow\downarrow}-n)!\,(n-1)!}. \tag{C3}$$

Hence for given values of $n_\uparrow$, $n_\downarrow$, and $n_\rightarrow$ the total number of different surfaces is

$$M(\mathbf{n},s_{\uparrow\downarrow}) = M_n(\mathbf{n})m(n_\uparrow,s_{\uparrow\downarrow})m(n_\downarrow,s_{\uparrow\downarrow}), \tag{C4}$$

and the total number of configurations with a given $s_{\uparrow\downarrow}$ and L, $M_{\text{tot}}(s_{\uparrow\downarrow},L)$, is given by summing $M(\mathbf{n},s_\uparrow)$ over all allowed configurations of $n_\uparrow$,$n_\downarrow$ and $n_\rightarrow$,

$$M_{\text{tot}}(s_{\uparrow\downarrow},L) = \sum_{n_\uparrow+n_\downarrow+n_\rightarrow=L} M(\mathbf{n},s_{\uparrow\downarrow}). \tag{C5}$$

A closed form solution exists for the restricted model where $n_{\uparrow\downarrow} = s_{\uparrow\downarrow}$, that is, we allow only steps of unit length. Applying the multinomial theorem yields $\tilde{M}_{\text{tot}}(L) = 3^L$. Since the model is restricted, there is an upper limit to s for a given L, which results in the number of configurations with size s being independent of s. This enables us to calculate the restricted partition function $\tilde{Z}$ easily as the sum of an infinite geometric series, and for a Hamiltonian of the form $H(s)/kT \sim \alpha s$, it yields simply $\tilde{Z} = 3^L/[1-\exp(-\alpha)]$.

[1] C. Alba-Simionesco, B. Coasne, G. Dosseh, G. Dudziak, K. E. Gubbins, R. Radhakrishnan, and M. Sliwinska-Bartkowiak, J. Phys.: Condens. Matter **18**, R15 (2006).

[2] W. C. Voorhees and P. W. Johnson, *Advances In Research And Applications*, Solid State Physics Vol. 59 (Elsevier, Amsterdam, 2004), p. 1.

[3] J. Gibbs, *The Scientific Papers of J. Willard Gibbs*, Vol. 1: Thermodynamics (Ox Bow, Woodbridge, CT, 1993).

[4] P. Müller and A. Saúl, Surf. Sci. Rep. **54**, 157 (2004).

[5] J. Tersoff and F. K. LeGoues, Phys. Rev. Lett. **72**, 3570 (1994).

[6] C. Misbah, O. Pierre-Louis, and Y. Saito, Rev. Mod. Phys. **82**, 981 (2010).

[7] J. G. Dash, A. W. Rempel, and J. S. Wettlaufer, Rev. Mod. Phys. **78**, 695 (2006).

[8] L. A. Rijniers, H. P. Huinink, L. Pel, and K. Kopinga, Phys. Rev. Lett. **94**, 075503 (2005).

[9] J.-P. Gratier, E. Frery, P. Deschamps, A. Røyne, F. Renard, D. K. Dysthe, N. Ellouz-Zimmerman, and B. Hamelin, Geology **40**, 1015 (2012).

[10] R. J. Flatt, F. Caruso, A. M. A. Sanchez, and G. W. Scherer, Nat. Commun. **5**, 4823 (2014).

[11] M. Schiro, E. Ruiz-Agudo, and C. Rodriguez-Navarro, Phys. Rev. Lett. **109**, 265503 (2012).

[12] J. Desarnaud, H. Derluyn, L. Molari, S. de Miranda, V. Cnudde, and N. Shahidzadeh, J. Appl. Phys. **118**, 114901 (2015).

[13] A. Putnis, Mineral. Mag. **66**, 689 (2002).

[14] J.-P. Gratier, D. K. Dysthe, and F. Renard, Adv. Geophys. **54**, 47 (2013).

[15] R. J. Asaro, W. A. Tiller, and S. Univer, Metall. Trans. **3**, 1789 (1972).

[16] M. A. Grinfeld, Sov. Phys. Dokl. **31**, 831 (1986).

[17] J. Bisschop and D. K. Dysthe, Phys. Rev. Lett. **96**, 146103 (2006).

[18] L. Angheluta, E. Jettestuen, J. Mathiesen, F. Renard, and B. Jamtveit, Phys. Rev. Lett. **100**, 096105 (2008).

[19] B. Derjaguin and L. Landau, Prog. Surf. Sci. **43**, 30 (1993).

[20] E. J. W. Verwey and J. T. G. Overbeek, *Theory of the Stability of Lyophobic Colloids* (Elsevier, Amsterdam, 1948).

[21] J. N. Israelachvili and G. E. Adams, J. Chem. Soc. Faraday Trans. 1 **74**, 975 (1978).

[22] I. K. Snook and W. van Megen, J. Chem. Phys. **72**, 2907 (1980).

[23] G. F. Becker and A. L. Day, Proc. Wash. Acad. Sci. **7**, 283 (1905).

[24] S. Taber, Am. J. Sci. **41**, 532 (1916).

[25] C. W. Correns, Discuss. Faraday Soc. **5**, 267 (1949).

[26] P. K. Weyl, J. Geophys. Res. **64**, 2001 (1959).

[27] M. Steiger, J. Cryst. Growth **282**, 455 (2005).

[28] L. G. Camara and F. Bresme, J. Chem. Phys. **119**, 2792 (2003).

[29] L. G. Cámara and F. Bresme, J. Chem. Phys. **120**, 11355 (2004).

[30] I. Kalcher and J. Dzubiella, Phys. Rev. E **88**, 062312 (2013).

[31] D. K. Dysthe, Y. Podladchikov, F. Renard, J. Feder, and B. Jamtveit, Phys. Rev. Lett. **89**, 246102 (2002).

[32] A. Røyne and D. K. Dysthe, J. Cryst. Growth **346**, 89 (2012).

[33] H. Yasuoka, R. Takahama, M. Kaneda, and K. Suga, Phys. Rev. E **92**, 063001 (2015).

[34] R. Renou, A. Szymczyk, and A. Ghoufi, Phys. Rev. E **91**, 032411 (2015).

[35] M. Degawa, T. J. Stasevich, W. G. Cullen, A. Pimpinelli, T. L. Einstein, and E. D. Williams, Phys. Rev. Lett. **97**, 080601 (2006).

[36] M. Degawa, T. Stasevich, A. Pimpinelli, T. Einstein, and E. Williams, Surf. Sci. **601**, 3979 (2007).

[37] W. Selke, Phys. Rev. E **90**, 012123 (2014).

[38] A. Voter, in *Radiation Effects in Solids*, NATO Science Series, Vol. 235 (Springer Netherlands, 2007), p. 1.

[39] J. N. Israelachvili, in *Intermolecular and Surface Forces* (Academic, San Diego, 2011), p. 291.

[40] C.-H. Lam, C.-K. Lee, and L. M. Sander, Phys. Rev. Lett. **89**, 216102 (2002).

[41] C.-H. Lam, Phys. Rev. E **81**, 021607 (2010).

[42] G. Russo and P. Smereka, J. Comput. Phys. **214**, 809 (2006).

[43] T. P. Schulze and P. Smereka, Commun. Comput. Phys. **10**, 1089 (2011).

[44] A. Chatterjee and D. G. Vlachos, J. Comput. Mater. Des. **14**, 253 (2007).
[45] G. Gilmer and P. Bennema, J. Cryst. Growth **13**, 148 (1972).
[46] R. J. Flatt, M. Steiger, and G. W. Scherer, Environ. Geol. **52**, 187 (2006).
[47] A. E. Flood, CrystEngComm **12**, 313 (2010).
[48] K. Machej, Chem. Eng. Process. **36**, 185 (1997).
[49] M. R. Khorsand, M. Habibian, N. Rohani, and A. R. Zarei, Iran. J. Chem. Chem. Eng. **29**, 13 (2010).
[50] P. Bennema and H. B. Klein Haneveld, J. Cryst. Growth **1**, 232 (1967).
[51] H. Haneveld, J. Cryst. Growth **10**, 111 (1971).
[52] P. M. Dove, N. Han, and J. J. De Yoreo, Proc. Natl. Acad. Sci. USA **102**, 15357 (2005).
[53] F. Salvatori, H. Muhr, E. Plasari, and J.-M. Bossoutrot, Powder Technol. **128**, 114 (2002).
[54] C. H. Donaldson, Mineral. Mag. **49**, 683 (1985).
[55] G. H. Gilmer, J. Appl. Phys. **43**, 1347 (1972).
[56] V. K. W. Cheng, J. Chem. Soc. Faraday Trans. **87**, 2467 (1991).